Effects of nano-YAG ($Y_3Al_5O_{12}$) crystallization on the structure and photoluminescence properties of Nd^{3+}-doped K_2O-SiO_2-Y_2O_3-Al_2O_3 glasses

Anal Tarafder, Atiar Rahaman Molla, Basudeb Karmakar*

Glass Science and Technology Section, Glass Division,
Central Glass and Ceramic Research Institute, Council of Scientific and Industrial Research (CSIR), 196, Raja S. C. Mullick Road, Kolkata 700 032, India

ABSTRACT

Nd^{3+}-doped precursor glass in the K_2O-SiO_2-Y_2O_3-Al_2O_3 (KSYA) system was prepared by the melt-quench technique. The transparent $Y_3Al_5O_{12}$ (YAG) glass-ceramics were derived from this glass by a controlled crystallization process at 750^oC for 5-100 h. The formation of YAG crystal phase, size and morphology with progress of heat-treatment was examined by X-ray diffraction (XRD), field emission scanning electron microscopy (FESEM), transmission electron microscopy (TEM) and Fourier transformed infrared reflectance spectroscopy (FT-IRRS). The crystallite sizes obtained from XRD are found to increase with heat-treatment time and vary in the range 35-45 nm. The measured photoluminescence spectra have exhibited emission transitions of $^4F_{3/2} \rightarrow {}^4I_J$ (J = 9/2, 11/2 and 13/2) from Nd^{3+} ions upon excitation at 829 nm. It is observed that the photoluminescence intensity and excited state lifetime of Nd^{3+} ions initially decrease and then gradually increase with increase in heat-treatment time. The present study indicates that the incorporation of Nd^{3+} ions into YAG crystal lattice enhance the fluorescence performance of the glass-ceramic nanocomposites.

Keywords: Transparent glass-ceramic, Nano-crystallized Nd^{3+}: YAG, Photoluminescence, Lifetime

* *Corresponding author. Tel.: +91 33 2473 3469; fax: +91 33 2473 0957.*
E-mail address: basudebk@cgcri.res.in (B. Karmakar).

1. Introduction

There are three reported synthetic crystalline phases of the yttria-alumina (Y_2O_3-Al_2O_3) composite phase diagram and yttrium aluminium garnet (YAG, $Y_3Al_5O_{12}$) is one of the most important crystal in that [1]. Other two are the yttrium aluminate monoclinic ($Y_4Al_2O_9$, YAM) and yttrium aluminum perovskite ($YAlO_3$, YAP). YAG possesses the cubic garnet structure (symmetry group: *Ia3d*) with eight formula units per unit cell. In the garnet lattice, the yttrium (Y^{3+}) ion is surrounded dodecahedrally by eight oxygen atoms and the aluminium (Al^{3+}) ion occupy both tetrahedral (four-fold) and octahedral (six-fold) coordination sites in a ratio of 3:2 [2]. Among the aforementioned three different phases, it is the only phase in the system which has excellent chemical, mechanical and thermal stability. Hence, single crystal YAG is an excellent creep resistant ceramic material and is an important high temperature engineering material used in structural refractory applications. Optically transparent single crystal YAG is also being used as optical host materials in various solid-state lasers for its outstanding optical properties when doped with lanthanide ($4f^{1-13}$) or transition ($3d^{1-9}$) elements. Laser operation of Nd-doped YAG single crystal fabricated by Czochralski method was first demonstrated by Geusic et al. [3] at Bell Laboratories in 1964. Since then it is one of the most widely used laser material available till date and is used for many different applications. Single crystal fabrication process has several disadvantages as an expensive Ir crucible is required for the growth of single crystal, and contamination from the crucible is hard to avoid. The low creep rate, high melting temperature (1940^{o}C), high oxidation resistance and low electrical conductivity make YAG particularly attractive for structural applications [4-8]. Relatively good structural properties combined with good optical properties render this material to be used in cathode-ray tube (CRTs), field emission displays (FED), scintillation and electro-luminescent applications as well [9-13].

In addition to its single crystal form, polycrystalline YAG doped with active rare-earth (RE) ions prepared by different routes other than glass-ceramics route has received much attention and has been used as an excellent phosphor or laser material [14-19]. However, the glass-ceramics route has not been used to prepare YAG based glass-ceramics laser materials. Johnson et al. [20] investigated kinetics and pathways for crystallization of glasses with YAG. Nishi et al. [21] investigated the phase-selective cathodoluminescence spectra of Er:YAG glass-ceramics. P. Jander [22] reported the crystallization of YAG in yttrium alumina silica glass and found that the crystallized phase was almost YAG but not transparent or nanocrystalline. Therefore, the reports of YAG based transparent glass-ceramics prepared by controlled crystallization of melt-quenched precursor glass are very rare. Moreover, in all the cases the derived glass-ceramics are macrocrystalline and opaque in nature, and are not suitable for optical applications.

During the past decades, the novel and enhanced properties of nanostructured materials have also attracted considerable attention for their interesting optical properties [23, 24]. In this context Tarafder el al. [25] and Chaliha et al. [26] have very recently reported the processing and properties of rare-earth (RE) doped nanostructured transparent glass-ceramics prepared by controlled crystallization technique. They have also reported that those nano glass-ceramics have potential optical applications. To the best of our knowledge, there is no report on transparent nanostructured YAG glass-ceramics in potassium aluminosilicate, K_2O-SiO_2-Y_2O_3-Al_2O_3 (KSYA) glass-matrix due to the difficulties in preparation of transparent precursor glass in general and transparent glass-ceramics in particular which involves high temperature (about 1650-1700^oC) for its precursor glass melting. In view of these, it is very interesting to study photoluminescence and other properties of Nd^{3+}-doped nanostructured and transparent YAG glass-ceramics prepared by controlled crystallization of precursor glass. These facts have motivated us to explore this opening.

Neodymium is one o the most widely studied luminescent ions emitting light especially for laser devices using the $^4F_{3/2} \rightarrow {}^4I_{11/2}$ transition at 1060 nm. Several works have been devoted to study Nd-doped optical glasses and crystal which have attracted much attention in the design of near-infrared solid state lasers. However, there is no report on the Nd-doped transparent YAG glass-ceramics.

In the present work, we report the preparation of Nd^{3+}-doped novel K_2O-SiO_2-Y_2O_3-Al_2O_3 (KSYA) based glass by melt-quench technique and transparent nano glass-ceramics by isothermal controlled crystallization of precursor glasses. The crystallization process has been studied by differential thermal analysis (DTA), X-ray diffraction (XRD), field emission scanning electron microscopy (FESEM), transmission electron microscopy (TEM) and Fourier transform infrared reflection spectroscopy (FT-IRRS). The glass and derived nano glass-ceramics were characterized by studying their thermal, structural and optical properties including near infrared (NIR) photoluminescence emissions and lifetimes,

2. Experimental procedures

2.1. Precursor glass preparation

The precursor glass having molar composition $28Ki_2O$-$42SiO_2$-$11.25Y_2O_3$-$18.75Al_2O_3$ doped with Nd_2O_3 (0.5 mol% in excess) was prepared from pure raw materials such as potassium carbonate, K_2CO_3 (GR, 99%, Loba Chemie, Mumbai, India), silica, SiO_2 (99.8%, Sipur A1 Bremtheler Quartzitwerk, Usingen, Germany), yttrium (III) oxide, Y_2O_3 (99.99%, Alfa Aesar, Ward Hill, MA), alumina, Al_2O_3 (99%, Aldrich, Milwaukee, WI), and neodymium (III) oxide, Nd_2O_3 (99.99%, Alfa Aesar, Ward Hill, MA) by conventional melt-quench technique. Here, the problem is that more quantity (> 30 mole%) of YAG forming oxides (Y_2O_3+Al_2O_3) incorporation in the $2K_2O$-$3SiO_2$ glass matrix was very difficult due to incomplete melting of the batch materials, inhomogeneity of the glass melt and finally

transformation the melt into a opaque mass after casting. Further it requires a melting temperature more than 1680^{o}C which is disagreeable in the context of use of platinum (melting point, 1768^{0}C) as melting crucible. The well-mixed batch, consisting of above raw materials, of about 150 g glass was melted in a platinum crucible in an electric furnace at 1680°C for 2h in air with intermittent stirring. The glass melt was poured onto a pre-heated iron mould. It was annealed at 700°C for 2 h to remove the internal stresses of the glass and then slowly cooled down to room temperature. The as-prepared glass block was cut into desired dimensions and optically polished for ceramization and subsequent characterization.

2.2. Characterization and measurements

The density of precursor glass was measured using Archimedes principle using water as buoyancy liquid. The refractive index of precursor glass was measured by a Prism Coupler (Model: 2010/M, Metricon Corporation, Pennington, NJ) at five different wavelengths (λ = 473, 532, 633, 1064 and 1552 nm). The coefficient of thermal expansion (CTE), glass transition temperature (T_g) and dilatometric softening temperature (T_d) of the precursor glass of cylindrical test sample (φ = 6 mm, L = 25 mm) was measured with an accuracy of ±1% using a horizontal-loading dilatometer (Model: DIL 402 PC, NETZSCH-Gerätebau GmbH, Selb, Germany) after calibration with a standard alumina supplied with the instrument by the manufacturer. The CTE in the temperature range 50-350^{o}C is reported here. XRD data were recorded using an XPERT-PRO MPD diffractometer (PANalytical, Almelo, the Netherlands) and the measurements were operated with Ni-filtered CuK_{α} = 1.5406 Å radiation as the X-ray source at 40 kV and 40 mA to identify the developed crystalline phases. The 2θ scan range was 10^{o} to 80^{o} with a step size of 0.05^{o}.

A high resolution FESEM (Gemini Zeiss Supra^{TM} 35 VP model of Carl Zeiss Microimaging GmbH, Berlin, Germany) was used to observe the microstructure of freshly

fractured surfaces of the heat-treated nano glass-ceramics after etching in 2% HF aqueous solution for 5 minutes, dried and then coated with a thin carbon film. The TEM images and selected area electron diffraction (SAED) of powdered glass-ceramic sample were obtained from FEI (Model: Tecnai G^2 30ST, FEI Company, Hillsboro, OR) instrument. The FT-IRRS of all Nd^{3+}-doped glass and glass-ceramic nanocomposites were recorded using a FTIR spectrometer (Model: 1615 Series, Perkin-Elmer Corporation, Norwalk, USA) in the wavenumber range 400-1500 cm^{-1} with a spectral resolution of $\pm$ 2 cm^{-1} and at 15^{o} angle of incidence. Optical absorption spectra were recorded UV-Vis-NIR spectrophotometer (Lambda 20, Perkin-Elmer Corporation, Norwalk, USA) at room temperature to monitor the changes of the environmental structure of the Nd^{3+} ions. The emission spectra were measured on an enhanced performance NIR continuous bench top modular spectrofluorometer (QuantaMaster, Photon Technology International, Birmingham, NJ) attached with Hamamatsu NIR-PMT (P1.7R) as detector and a Xe arc lamp as excitation source. The excited state lifetime was measured with the same instrument using a Xe flash lamp of 75 W.

3. Results and discussion

3.1. Thermal, optical and other physical properties

The composition of precursor glass is $28Ki_2O$-$42SiO_2$-$11.25Y_2O_3$-$18.75Al_2O_3$ (mol%) doped with 0.5 mol% Nd_2O_3 (in excess). In our preliminary experimentation, we had tried to melt several glass compositions containing higher quantities of YAG forming oxides (Y_2O_3 and Al_2O_3). But, it is observed that incorporation of higher quantity (>30 mol%) of Y_2O_3 and Al_2O_3 in the glass matrix without sacrificing the transparency was difficult. In this context it may be mentioned that Nishi et al. [21] could incorporate 29.5 mol% YAG compositions in the $34CaO$-$8.5Y_2O_3$-$21Al_2O_3$-$36SiO_2$-$0.5Er_2O_3$ glass-matrix. However, their ultimate glass-ceramic was opaque. Another problem in this respect is that the incorporation of more

quantity (>30 mole%) of (Y_2O_3+Al_2O_3) requires higher melting temperature (>1680^oC) which is detrimental in the view of use as solid state lasers because of the fact of inclusion of platinum increases with increase in melting temperature of glass [27] as well. The coefficient of thermal expansion (CTE), glass transition temperature (T_g) and dilatometric softening point (T_d) of the precursor was measured using a dilatometer and the measured values from the dilatometric curve (Fig. 1) are presented in Table 1. CTE was measured over the temperature range of 50- 350^0C and its value is 109 x 10^{-7} K^{-1}. The dilatometric curve revealed that the precursor glass possesses a very high glass transition (815^0C) and softening temperature (864^0C) due to the presence of high melting SiO_2, Y_2O_3 and Al_2O_3 as major constituents of glass.

The precursor glass is visually transparent, appearing blue purple due to Nd^{3+} doping. The precursor glass samples were heat treated at 750^oC for 5, 10, 20, 50 and 100 h after nucleating at 700^oC for 2 h. The obtained samples were labelled as a, b, c, d, e and f (Fig. 2) respectively for convenience. Details are given in Table 2. In the preliminary experimentation to obtain nanostructured transparent glass-ceramics, it was observed that the precursor glass had been transformed into opaque glass-ceramics after heat-treating at T_g or above T_g. In the course of this investigation, we established an optimum nucleation temperature of 700^oC and crystallization temperature of 750^oC where the nano glass-ceramics maintain their transparency. Tarafder et al. [28] has also adopted a similar heat-treatment protocol for developing nanostructured transparent Eu^{3+}:$LiTaO_3$ in Li_2O-Ta_2O_5-SiO_2-Al_2O_3 glass-ceramics. The transparency of the precursor glass persists in heat-treated samples. The blue purple color intensity decreases with progress of heat-treatment duration due to devitrification and the resultant glass-ceramics thus obtained became less transparent. The measured density of the precursor glass is 3.031 $g.cm^{-3}$ and this high value attributes to the presence of high molecular weight Y_2O_3 as a component of the glass. Fig. 3 presents Cauchy

fitting based on measured refractive indices at five different wavelengths (see experimental techniques) and shows the dependences of the refractive index on the wavelength for precursor glass (a) and the 10 h heat-treated glass-ceramics (c) sample. In general, refractive index decreases with increasing wavelength due to dispersion. This trend is observed in both the samples. In addition to this, the refractive index of the glass-ceramic sample (c) has increased in comparison with precursor glass (a) that can be seen in Fig. 3. The refractive indices n_F, n_D and n_C have been estimated at three standard wavelengths (λ_F = 486.1 nm, λ_D = 589.2 nm and λ_C = 656.3 nm respectively) from the dispersion curve (Fig. 3, curve a). The Abbe number (υ_D) is calculated by the relation

$$\upsilon_D = \frac{n_D - 1}{n_F - n_C} \tag{1}$$

The calculated υ_D for precursor glass (a) and glass-ceramic (c) are 46 and 47 respectively. Therefore, the glass-ceramics are of lower dispersion than precursor glass. The average molar refraction (R_m) presented in Table 1 were calculated from Lorentz-Lorentz equation [29]:

$$R_m = [(n^2 - 1)/n^2 + 2)]V_m \tag{2}$$

and the molar electronic polarizability (α_m) is calculated as [29-31]:

$$\alpha_m = \frac{3R_m}{4\pi N_A} \tag{3}$$

where V_m is the molar volume ($V_m = M_{av}/\rho$), M_{av} is the average molecular weight, ρ is the density, n is the refractive index at wavelength λ_D = 589.2 nm evaluated from the dispersion curve (Fig. 3, curve a), and N_A is Avagadro's number.

We have calculated the concentration (N_{RE}) of Nd^{3+} ions/cm^3 and the distance between rare-earth species (mean inter-ionic distance, R_i) as [32]

$$N_{RE}(ions/cm^3) = (A.N_A.\rho)/M_{av} \quad (4)$$

$$R_i(\overset{o}{A}) = (1/N_{Nd^{3+}})^{1/3} \quad (5)$$

It is observed that the formation of high refractive index YAG (RI = 1.8317 at 600 nm [33]) causes the heat-treated sample to exhibit higher refractive indices as compared to precursor glass. This is shown in Fig. 3, curve-c.

3.2. X-ray diffraction analysis

The X-ray diffraction pattern of the Nd^{3+}-doped KSYA precursor glass and cerammed glass-ceramics are shown in Fig. 4. No diffraction peak appears for the samples a-b which indicates that the powders are amorphous in nature for these samples. The diffraction peak of the samples d-f heat-treated for longer duration are indexed and it resembled to some extent as $Y_3Al_5O_{12}$ phase (JCPDS file 33-0040). Progression of heat-treatment leads to an increase of diffraction peak intensity and a decrease of peak full-width at half-maxima (FWHM) due to the improved crystallinity and the coarsening of grains.

From the full width at half maximum (FWHM) of the most intense diffraction peak (420) of transparent YAG nano glass-ceramics, the average crystallite size (diameter, *d*) is calculated by using the Scherrer's formula [34]

$$d = 0.9\lambda/\beta\cos\theta \quad (6)$$

where λ is the wavelength of X-ray radiation (CuK_α = 1.5406Å), β is the full width at half maximum (FWHM) of the peak at 2θ.

The average calculated crystallite sizes of YAG nanocrystal increase with progression of heat-treatment and the values increasing from 25-40 nm over the investigated heat-treatment

time period. It is observed from the XRD diagram that there is evidence of presence of minor amount $KAlSiO_4$ (JCPDS file 33-0989) in some of the derived glass-ceramic nanocomposites which is also marked in Fig. 4.

3.3. FESEM and TEM image analyses

The size, shape and morphology of glass-ceramic nanocomposites were studied by FESEM and TEM analyses. FESEM images of the polished surface of samples c and f have been presented in Figs. 5(a) and (b) respectively. The FESEM micrographs point towards the phase separation of glassy matrix with heat-treatment time and followed by incipient precipitation of defined crystallites within the phase-separated grains with increase in heat-treatment time. The phase separated grains are irregular in shapes and distributed thought out the bulk glass matrix. The size of the phase separated grains varies in the range 40-60 nm. These grains are well separated and grown with distinct features by way of further increase in heat-treatment time (Fig. 5 b). Comparing with the crystallite sizes, it is clear that these grains are polycrystalline in nature. Fig. 6 shows bright field TEM image of glass-ceramic nanocomposites (f) and its inset shows the selected area electron diffraction (SAED) pattern from the dotted encircled region. The SAED pattern confirms the presence of crystalline YAG in the glass-ceramic nanocomposites as JCPDS file 33-0040. It is also found that the crystallite sizes are in the range of 20-30 nm.

3.4. Fourier transform infrared reflectance spectroscopy (FTIRRS)

The FT-IRRS of the bulk precursor glass and heat-treated samples in the wavenumber range 400-1500 cm^{-1} are shown in Fig. 7. It is seen from this figure that the precursor glass (curve-a) exhibits three broad reflection bands centred around 950, 675 and 475 cm^{-1} as a result of wider distribution of silicon and YAG structural units. It is also observed that one

more reflection band gradually appeared around 575 cm^{-1} with increasing heat-treatment duration. The reflection bands centred at 690, 575 and 475 cm^{-1} are assigned to the characteristics Al-O and Y-O band vibrations of crystalline YAG. All these bands well matched with the reported data of a crystallized YAG [35-38]. The reflection band centred at 950 cm^{-1} and gradually shifted to 990 cm^{-1}. It is assigned to Si-O stretching vibration of residual glass and potassium aluminium silicate [39]. It is seen that with progression of heat-treatment all the FTIR reflection band intensities increase and become narrower gradually. Thus from the investigations of FTIR reflectance spectra of Nd^{3+} doped K_2O-SiO_2-Y_2O_3-Al_2O_3 glass and glass-ceramics, it is observed that the crystallization is taking place of mainly YAG crystal along with minor quantity of potassium aluminum silicate phase formation in the residual glass matrix. The results of the FT-IRRS are in good agreement with that of XRD and FESEM studies.

3.5. UV-visible-NIR absorption spectra analyses

The room temperature measured absorption spectra of the Nd^{3+}-doped precursor glass (a) and 5, 10, 50 and 100 h heat-treated glass-ceramic samples (b, c, e and f respectively) in the UV-visible-NIR range (300-900 nm) have been presented in Fig. 8. The spectra reveal absorption peaks due to the $4f^3$-$4f^3$forced electric dipole transitions from the ground $^4I_{9/2}$ state to different excited states of Nd^{3+} ion in $4f^3$ configuration. All the peaks $^4I_{9/2} \rightarrow {}^4D_{3/2}$ (351 nm), $^4I_{9/2} \rightarrow {}^4D_{1/2}$ (359 nm), $^2P_{1/2}$ (431 nm), $^2G_{9/2}$ (474 nm), $^4G_{9/2}$ (514 nm), $^4F_{9/2}$ (684 nm), $^4F_{7/2}$+$^4S_{3/2}$ (741 nm), $^4F_{5/2}$+$^2H_{9/2}$ (808 nm) and $^4F_{3/2}$ (881 nm) are assigned in accordance with Carnall's convention [40, 41]. From this figure it is noticed that the base line of absorption spectra of heat-treated samples (b, c, e and f) has been elevated significantly with the diminishing intensities of the absorption peaks. This uplifting can be attributed to scattering of short wavelength light by the crystals [42, 43] or may be due to the difference in refractive index of crystalline phase (RI of YAG is 1.8317 at 600 nm [33] with that of

residual glassy matrix (RI = 1.5887 at 656.3 nm, see Table 1). Since the crystallites (14-36 nm) are smaller than the visible wavelength, a Rayleigh scattering model should be applicable [44]. According to this model, the scattering loss, τ is given by

$$\tau = \frac{32\pi^4 d^3 (n\Delta n)^2}{3\lambda^4} NV \qquad (7)$$

where d is the particle diameter, λ the wavelength of light, n the refractive index, N the number density of particles, and V the volume of the particle. With progression of heat-treatment, the number and sizes of nanocrystallites developed in the glassy matrix increase and hence the scattering centre and scattering loss increase that corresponds to a decrease in the visible transparency of the glass-ceramic nanocomposites. There is no significant difference in the shapes of absorption bands for glass and crystallized sample.

3.6. NIR excited NIR emission and excitation spectra analyses

The emission spectra of the precursor glass and the glass-ceramic nanocomposites under the excitation at 829 nm monochromatic light from an arc Xe lamp is shown in Fig. 9(A). Fig. 9(B) shows their excitation spectra measured in the wavelength range 300–950 nm by monitoring with the intense NIR emission located at 1069 nm. The emission spectra of the Nd^{3+}-doped glass (a) and the glass–ceramic nanocomposites exhibit three emission peaks at 904, 1069 and 1343 nm. These three emission peaks can be attributed to the $^4F_{3/2} \rightarrow {}^4I_{9/2}$, $^4I_{11/2}$, $^4I_{13/2}$ transitions of Nd^{3+} respectively. The main emission peak near 1069 nm is assigned to the $^4F_{3/2} \rightarrow {}^4I_{11/2}$ of Nd^{3+}. The emission band intensity around 1069 nm decreases with progression of heat-treatment. This decrease in emission intensity is due to the clustering of Nd^{3+} ions which is extremely sensitive to concentration quenching [45]. Dejneka [46] has demonstrated in fluoride glasses that clustering thereby quenching occurs when the Eu^{3+}-Eu^{3+}

ionic separation is around 40 Å. In the present case, the Nd^{3+}-Nd^{3+} ionic separation (R_i) in the precursor glass is found to be about 38 Å which was calculated using the equation 5. It is, therefore, seen that the Nd^{3+}- Nd^{3+} ionic separation (R_i) is in the quenching region. Theoretically, the rate of relaxation due to concentration quenching varies as R_i^{-6} [32, 47, 48]. With the progress of heat-treatment, the YAG crystal phase has been formed and the Nd^{3+} ions partitioned into the residual glassy phase by reducing the inter-ionic separation less than 38 Å of precursor glasses. This fact results in reduction in fluorescence intensity (see curve: b-f, Fig. 9(A)) due to concentration quenching. The emission bands become sharper and take shapes as in crystalline host with progress of heat-treatment duration. It has also been observed from the emission spectra that the emission intensity ratio ($^4F_{3/2}\rightarrow{}^4I_{11/2}$)/($^4F_{3/2}\rightarrow{}^4I_{9/2}$) of Nd^{3+} ions increases with progression of heat-treatment, then becomes almost constant after a certain time and the same has been presented in Fig. 10. This is significant from the point of view of 1.06 μm laser applications.

3.7. Lifetime

Figure 11 shows the room temperature fluorescence decay curves for Nd^{3+} ions in precursor glass (a) and nano glass-ceramics (d and f) of the emission transition ($^4F_{3/2}\rightarrow{}^4I_{11/2}$) at 1069 nm with an excitation at 829 nm. The measured curves demonstrate a single exponential decay. The excited state lifetime (τ_f) for all has been estimated from these decay curves and the results are shown in Table 3. It is seen that the excited state ($^4F_{3/2}$) lifetime (τ_f) increases with increase in Nd^{3+}:YAG nanocrystallite sizes. Such variation can be attributed to the high interaction of smaller particles with the high energy phonons of surrounding silicate glass (about 1100 cm^{-1}) which increases the nonradiative relaxation with decrease in particle size [49]. In larger particles, less interaction with surrounding glass along with stable crystal site occupation by the Nd^{3+} ion in the low phonon energy YAG host (about 690 cm^{-1} of YAG

nanocrystal, see Fig. 5(a) decrease the nonradiative relaxation and thereby increase the measured lifetime (τ_f) as governed by the equation [50]:

$$\tau_f = \frac{1}{A_{rad} + W_{nr}} \quad (8)$$

where A_{rad} and W_{nr} are the radiative and nonradiative rates respectively. A similar observation has earlier been reported by Tarafder et al. [25].

4. Conclusions

The thermal, structural and optical properties of Nd_2O_3 doped transparent glass and glass-ceramic nanocomposites in the K_2O-SiO_2-Y_2O_3-Al_2O_3 system are demonstrated here. The results of XRD, FESEM, TEM and FT-IRRS evidenced the formation of nanocrystalline YAG phase in the KSYA glass matrix. The nanocrystallite size of YAG has been evaluated from XRD, and found to vary in the range 35-45 nm. The FESEM images indicate that with progress of heat-treatment crystallization of nano YAG takes place in phase separated grains preceding by a phase separation mechanism. TEM image also revealed that the crystallite size varies in the range of 30-40 nm. The appearance of Al-O and Y-O vibration lines in FTIR reflection spectra is also characteristics to this YAG phase transition. It is our belief that this work would generate new knowledge base in the area of YAG glass-ceramic nanocomposites.

Acknowledgements

This research was supported by the institute as an in-house project under the project no. OLP0270. The authors thank Prof. Indranil Manna, Director of the institute for his kind

permission to publish this paper. They thank Dr. R. Sen, Head, Glass Division, CGCRI for his encouragement to carry out this work. The authors would like to thank Dr. K. Annapurna and Dr. Kaushik Biswas, Scientists, CGCRI for their help in recording the photoluminescence and refractive indices respectively. They also thankfully acknowledge XRD and Electron Microscope Divisions of this institute for recording XRD patterns and microscopic images respectively.

References

[1] J. S. Abell, R. Harris, B. Cockayne, B. Lent, J. Mater. Sci. 9 (1974) 527–537.

[2] C. Landron, S. Lefloch, M. Gervais, J. P. Coutures, phys. Stat. Sol. 196 (1996) 25-31.

[3] J. E. Geusic, H. M. Marcos, L. G. Van Uitert, Appl. Phys. Lett. 4 (1964)182-184.

[4] B. H. King, J. W. Halloran, J. Am. Ceram. Soc. 78 (1995) 2141-2148.

[5] Y. Liu, Z. F. Zhang, J. Halloran, R. M. Laine, J. Am. Ceram. Soc. 81(1998) 629-645.

[6] W. R. Blumenthal, D. S. Phillips, J. Am. Ceram. Soc. 79 (1996) 1047-1052.

[7] J. K. R. Weber, B. Cho, A. D. Hixson, J. G. Abadie, P. C. Nordine, W. M. Kriven, B. R. Johnson, D. Zhu, J. Eur. Ceram. Soc. 19 (1999) 2543-2550.

[8] P. A. Doleman, E. G. Butler, Key Engng. Mater. 127–131 (1997)193-202.

[9] S. M. Sim, K. A. Keller, T. I. Mah, J. Mater. Sci. 35 (2000) 713–716.

[10] X. D. Zhang, H. Liu, W. He, J. Y. Wang, X. Li, R. I. Boughton, J. Alloys Compd. 372 (2004) 300–303.

[11] Y. H. Zhou, J. Lin, M. Yu, S. M. Han, S. B. Wang, H. J. Zhang, Mater. Res. Bull. 38 (2003) 1289–1299.

[12] X. Li, H. Liu, J. Y. Wang, H. M. Cui, X. D. Zhang, F. Han, Mater. Sci. Eng. A 379 (2004) 347–350.

[13] R. A. Rodriguez, E. De la Rosa, L. A. Diaz-Torres, P. Salas, R. Melendrez, M. Barboza-Flores, Opt. Mater. 27 (2004) 293–299.

[14] Z. Wu, X. Zhang, W. He, Y. Du, N. Jia, G. Xu, J. Alloys. Compd. 468 (2009) 571-574.

[15] S. Fujita, A. Sakamoto, S. Tanabe, IEEE Sel. Top. Quantum Electron. 14 (2008) 1387-1391.

[16] G. Xia, S. Zhou, J. Zhang, J. Xu, J. Cryst. Growth 279 (2005) 357-362.

[17] D. Boyer, G. B. Chadeyron, R. Mahiou, Opt. Mater. 26 (2004) 101-105.

[18] S. Nakamura, H. Yoshioka, Y. Matsubara, T. Ogawa, S. Wada, Opt. Commun. 281 (2008) 4411-4414.

[19] J. Lu, M. Prabhu, J. Song, C. Li, J. Xu, K. Ueda, A. A. Kaminskii, H. Yagi, T. Yanagitani, Appl. Phys. B 71 (2000) 469-473.

[20] B. R. Johnson, W. M. Kriven, J. Mater. Res. 16 (2001) 1795-1805.

[21] M. Nishi, S. Tanabe, K. Fujita, K. Hirao, G. Pezzotti, Solid State. Commun. 132 (2004) 19-23.

[22] P. Jander, Ph.D. Thesis, "An Investigation of Novel Materials for Active Optical Devices," Optoelectronics Research Centre, Faculty of Engineering and Applied Science, University of Southampton, UK, Dec. 2002.

[23] R.N. Bhargava, D. Gallagher, X. Hong, A. Nurmikko, Phys. Rev. Lett. 72 (1994) 416-419.

[24] G. Xia, S. Zhou, J. Zhang, S. Wang, Y. Liu, J. Xu, J. Cryst. Growth 283 (2005) 257–262.

[25] A. Tarafder, K. Annapurna, R. S. Chaliha, V. S. Tiwari, P. K. Gupta, B. Karmakar, J. Am. Ceram. Soc. 92 (2009) 1934-1939.

[26] R. S. Chaliha, K. Annapurna, A. Tarafder, V. S. Tiwari, P. K. Gupta, B. Karmakar, Solid State Sci. 11 (2009) 1325–1332.

[27] J. S. Hayden, A. J. Marker III, Metal Inclusion: Platinum, in Analysis of the Composition and Structure of Glass and Glass Ceramics, pp. 491-496, Edited by H. Bach and D. Krause, Springer-Verlag, Berlin, 1999.

[28] A. Tarafder, K. Annapurna, R. S. Chaliha, V. S. Tiwari, P. K. Gupta, B. Karmakar, J. Mater. Sci. 44 (2009) 4495–4498.

[29] H. Scolze, Glass Nature, Structure and Properties, p. 145, Springer, New York, 1991.

[30] V. Dimitrov, T. Komatsu, J. Solid State Chem. 163 (2002) 100.

[31] V. Dimitrov, T. Komatsu, J. Solid State Chem. 178 (2005) 831.

[32] K. Patek, Glass Lasers, Butterworth & Co. (Publishers) Ltd., London, 1970.

[33] D. E. Zelmon, D. L. Small, R. Page, Appl. Optics 37 (1998) 4933-4935.

[34] B. D. Cullity, Elements of X-Ray Diffraction, 2nd Edition, pp. 101-2, Addison-Wesley Publishing Co., London, 1978.

[35] A. M. Hofmeister, K. R. Campbell, J. Appl. Phys. 72 (1992) 638-646.

[36] L. M. Seaverson, S. Q. Luo, P. L. Chien, J. F. McClelland, J. Am. Ceram. Soc. 69 (1986) 423-429.

[37] P. Apte, H. Bruke, H. Pickup, J. Mater. Res. 7 (1992) 706-711.

[38] Q. Lu, W. Dong, H. Wang, X. Wang, J. Am. Ceram. Soc. 85 (2002) 490-492.

[39] G. Fuxi, Optical and Spectroscopic Properties of Glass, pp. 18-61, Springer-Verlag, Berlin, 1992.

[40] W. T. Carnall, P. R. Fields, K. Rajnak, J. Chem. Phys. 49 (1968) 4450-4455.

[41] A. Ivankov, J. Seekamp, W. Bauhofer, J. Lumin. 121 (2006) 123-131.

[42] G. H. Beall, D. A. Duke, Glass-Ceramic Technology in Glass Science and Technology; Vol. 1, p.403, Edited by D. R. Uhlmann and N. J. Kreidl, Academic Press, New York, 1983.

[43] G. H. Beall, D. A. Duke, J. Mater. Sci. 4 (1969) 340-352.

[44] H. C. Van De Hulst, Light Scattering by Small Particles, Wiley, New York, 1957.

[45] P. Riello, S. Bucella, L. Zamengo, U. Anselmi-Tamburini, R. Francini, S. Pietrantoni, Z. A. Munir, J. Eur. Ceram. Soc. 26 (2006) 3301.

[46] M. J. Dejneka, J. Non-Cryst. Solids 239 (1998) 149.

[47] J. H. Campbell, T.I. Suratwala, J. Non-Cryst. Solids 263–264 (2000) 318.

[48] U. Kang, A.A. Zhilin, D.P. Logvinov, A.A. Onushchenko, V.A. Savost'yanov, T.I. Chuvaeva, A.V. Shashkin, Glass Phys. Chem. 27 (2001) 344.

[49] R. S. Meltzer, W. M. Yen, H. Zheng, S. P. Feofilov, M. J. Dejneka, Phys. Rev. B 66 (2002) 224202 (1-6).

[50] M. Yamane, Y. Asahara, Glasses for Photonics, Cambridge University Press Cambridge, UK, 2000.

Figure Captions

Fig. 1. Dilatometric curve of (a) Nd^{3+}:K_2O-SiO_2-Y_2O_3-Al_2O_3 precursor glass.

Fig. 2. (Color online) Photograph of (a) Nd^{3+}:YAG precursor glass and (b-f) glass-ceramic nanocomposites (thickness: 2 mm) obtained after heat-treatment for different duration at 750^0C laid over the writing to show their transparency. (See Table 2 for sample identity)

Fig. 3. (Color online) Variation of refractive indices (Cauchy fitted) as a function of wavelength of Nd^{3+}:YAG (a) precursor glass and (c) glass-ceramic nanocomposites obtained after 10 h heat-treatment at 750^0C. (See Table 2 for sample identity)

Fig. 4. XRD patterns of the (a) precursor glass and (b-f) glass-ceramic nanocomposites (for details see Table 2).

Fig. 5. FESEM images of samples (a) c and (b) e (for details see Table 2).

Fig. 6. TEM image of glass ceramic nanocomposites f and inset shows the SAED pattern from the dotted encircled region (for details see Table 2).

Fig. 7. FT-IRR spectra of precursor glass (a), and glass-ceramic nanocomposites (d) and (f). (For details see Table 2)

Fig. 8. (Color online) Absorption spectra of samples a-c and e-f (thickness: 2 mm, for details see Table 2).

Fig. 9. (Color online) (A) NIR fluorescence spectra (λ_{ex} = 829 nm) of Nd^{3+}:YAG precursor glass and glass-ceramic nanocomposites b-f obtained after heat-treatment for various duration and (B) Excitation spectra of sample a, c, d, and f. (For details see Table 2)

Fig. 10. Emission intensity ratio ($^4F_{3/2} \rightarrow {}^4I_{11/2}$)/($^4F_{3/2} \rightarrow {}^4I_{9/2}$) of Nd^{3+} ions in precursor glass and glass-ceramic nanocomposites with increase of heat-treatment time. (For details see Table 2)

Fig. 11. (Color online) Decay curves for the $^4F_{3/2} \rightarrow {}^4I_{11/2}$ transition of Nd^{3+} ion at 1069 nm under excitation at 829 nm of samples a, d, and f. (For details see Table 2)

Table 1
Some measured and calculated properties of Nd^{3+} doped precursor glass

Properties	Corresponding value
Average molecular weight, M_{av}	97.327
Density, ρ ($g.cm^{-3}$)	3.031
Refractive indices:	
n_F (at 486.1 nm)	1.6015
n_D (at 589.2 nm)	1.5925
n_C (at 656.3 nm)	1.5887
Abbe number (υ_D)	46
Dispersive power (υ_D^{-1})	0.02
Molar refractivity, R_M (cm^3)	10.87
Electronic polarizability, α (cm^3)	4.31×10^{-24}
Nd^{3+} ion concentration, $N_{Nd^{3+}}$ ($ions.cm^{-3}$)	1.87×10^{22}
Nd^{3+}-Nd^{3+} inter ionic distance, R_i (Å)	38
Crystallization peaks, T_{p1} and T_{p2} (^0C)	940 and 971
CTE, α, (50-350^{0}C) x 10^{-7} K^{-1}	109
Glass transition temperature, T_g (^0C) (DTA)	821
Glass transition temperature, T_g (^0C) (Dil.)	815
Dilatometric softening temperature, T_d (^0C)	864

Table 2
Preparative conditions and crystallinity of glass-ceramic nanocomposites

Sample identity	Heat-treatment time (h) at 750^{o}C	Crystallinity
a	0	Amorphous
b	5	Amorphous
c	10	$Y_3Al_5O_{12}$
d	20	$Y_3Al_5O_{12}$
e	50	$Y_3Al_5O_{12}$ + $KAlSiO_4$ (very minor)
f	100	$Y_3Al_5O_{12}$ + $KAlSiO_4$ (very minor)

Table 3
Measured lifetime, Emission intensity ratio ($^4F_{3/2}\rightarrow{}^4I_{11/2}$)/($^4F_{3/2}\rightarrow{}^4I_{9/2}$) and FT-IRRS intensity of precursor glass (a) and glass-ceramic nanocomposites (d) and (f)

Sample identity	Lifetime, τ (μs)	Emission intensity ratio, ($^4F_{3/2}\rightarrow{}^4I_{11/2}$) /($^4F_{3/2}\rightarrow{}^4I_{9/2}$)	FT-IRRS[a] intensity (I_{YAG})	
			690 cm^{-1}	475 cm^{-1}
a	256	1.854	7.51	13.40
d	244	2.370	7.87	15.77
f	242	2.613	9.07	21.20

[a]FT-IRRS, Fourier transformed infrared reflectance spectroscopy.

Figures

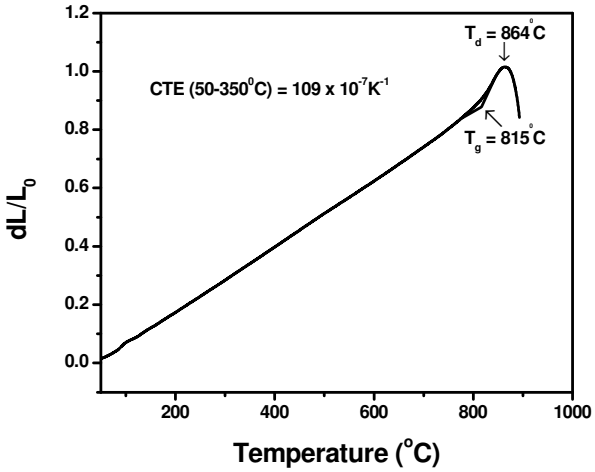

Fig. 1. Dilatometric curve of (a) Nd^{3+}:K_2O-SiO_2-Y_2O_3-Al_2O_3 precursor glass.

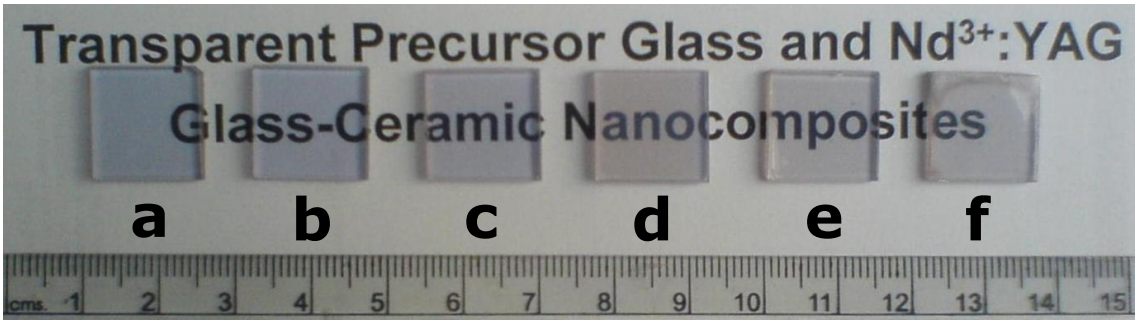

Fig. 2. (Color online) Photograph of (a) Nd^{3+}:YAG precursor glass and (b-f) glass-ceramic nanocomposites (thickness: 2 mm) obtained after heat-treatment for different duration at 750^0C laid over the writing to show their transparency. (See Table 2 for sample identity)

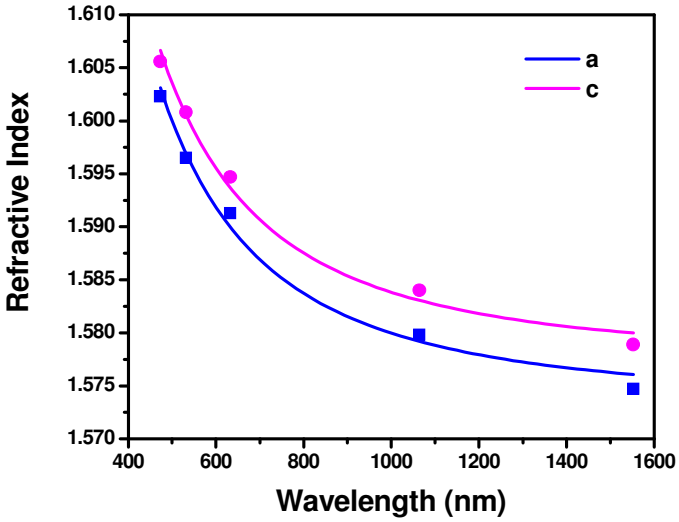

Fig. 3. (Color online) Variation of refractive indices (Cauchy fitted) as a function of wavelength of Nd^{3+}:YAG (a) precursor glass and (c) glass-ceramic nanocomposites obtained after 10 h heat-treatment at 750^0C. (See Table 2 for sample identity)

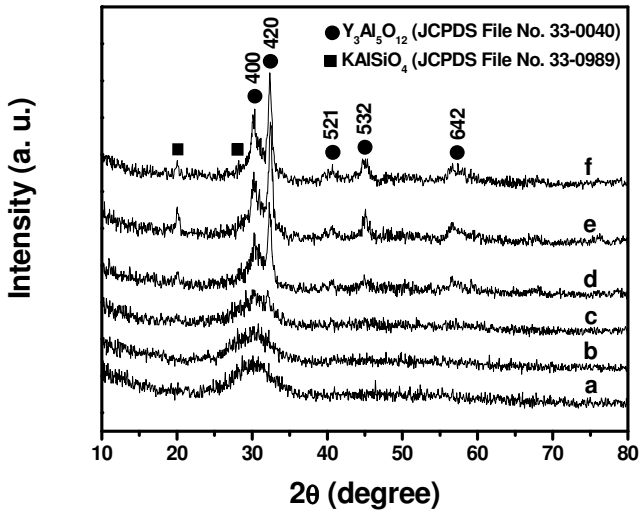

Fig. 4. XRD patterns of the (a) precursor glass and (b-f) glass-ceramic nanocomposites (for details see Table 2).

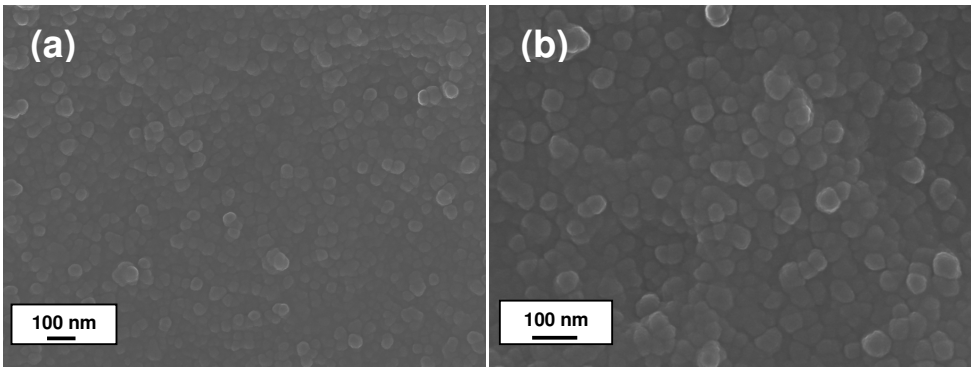

Fig. 5. FESEM images of samples (a) c and (b) e. (For details see Table 2)

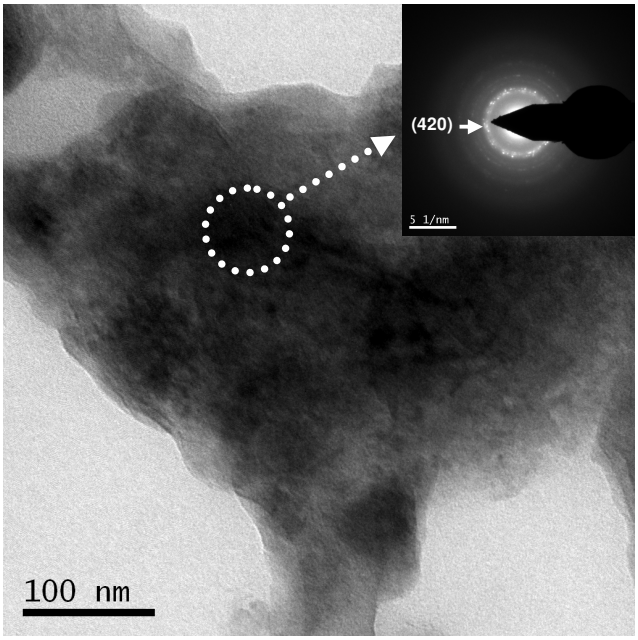

Fig. 6. TEM image of glass ceramic nanocomposites f and inset shows the SAED pattern from the dotted encircled region (for details see Table 2).

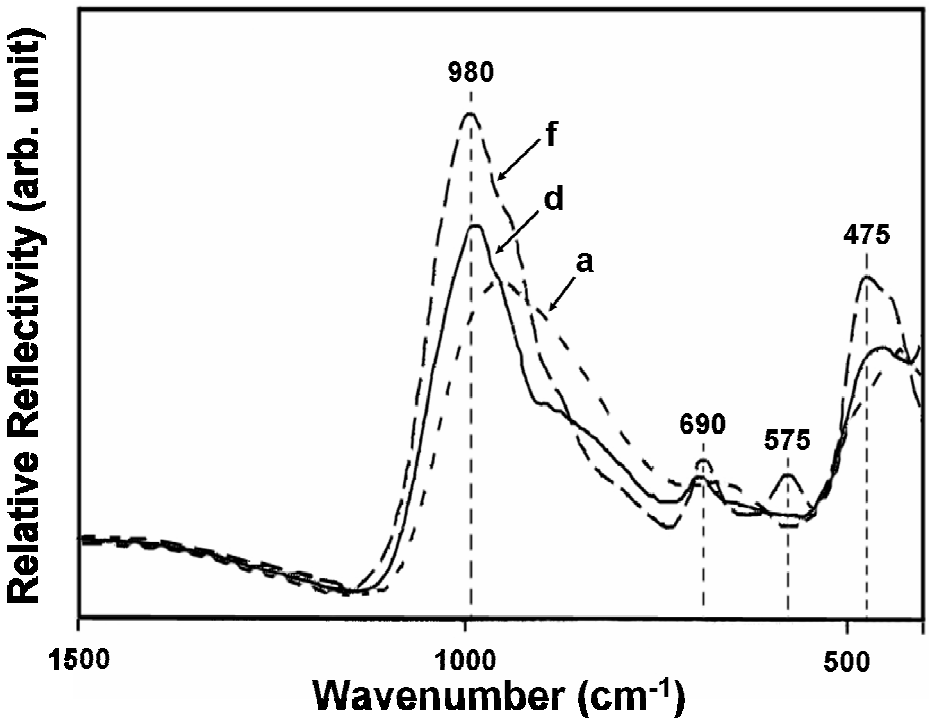

Fig. 7. FT-IRR spectra of precursor glass (a), and glass-ceramic nanocomposites (d) and (f). (For details see Table 2)

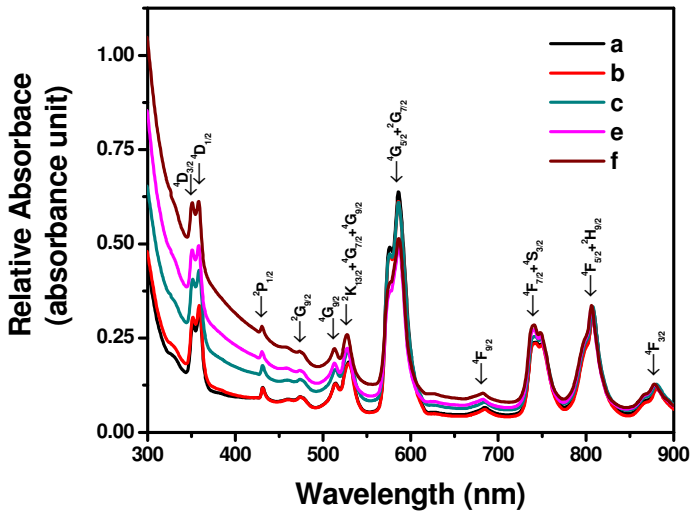

Fig. 8. (Color online) Absorption spectra of samples a-c and e-f (thickness: 2 mm, for details see Table 2).

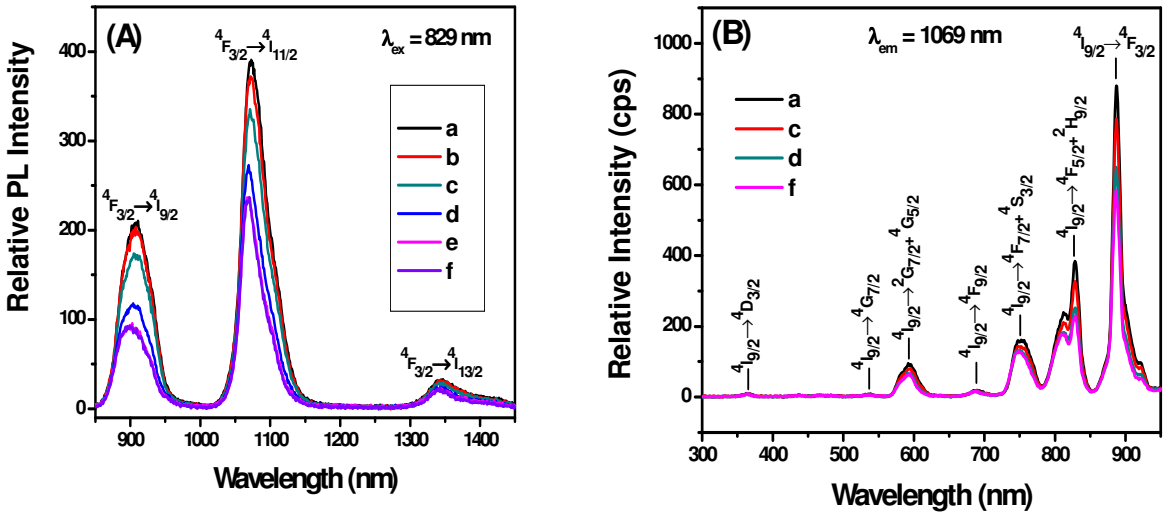

Fig. 9. (Color online) (A) NIR fluorescence spectra (λ_{ex} = 829 nm) of Nd^{3+}:YAG precursor glass and glass-ceramic nanocomposites b-f obtained after heat-treatment for various duration and (B) Excitation spectra of sample a, c, d, and f. (For details see Table 2)

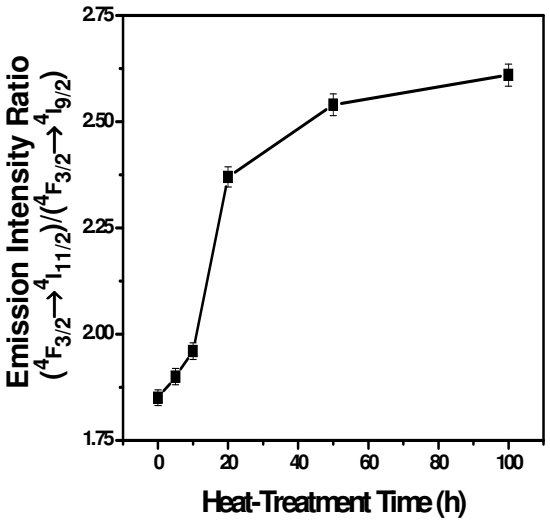

Fig. 10. Emission intensity ratio ($^4F_{3/2}\rightarrow{}^4I_{11/2}$)/($^4F_{3/2}\rightarrow{}^4I_{9/2}$) of Nd^{3+} ions in precursor glass and glass-ceramic nanocomposites with increase of heat-treatment time. (For details see Table 2)

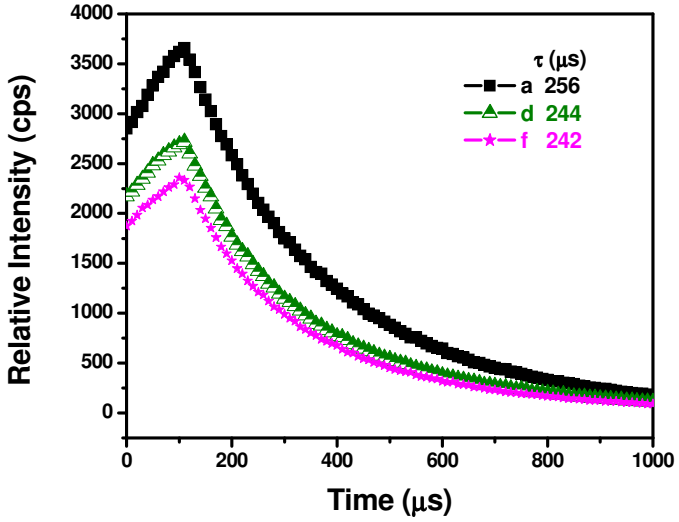

Fig. 11. (Color online) Decay curves for the $^4F_{3/2} \rightarrow {}^4I_{11/2}$ transition of Nd^{3+} ion at 1069 nm under excitation at 829 nm of samples a, d, and f. (For details see Table 2)